

## Supplementary Materials

Based on the k·p perturbation method, in Sec. (S1) we derive the effective Hamiltonian for the bilayer sonic crystal (BSC) in the vicinity of the Brillouin zone corners K and K'. Specifically, the K valley is focused and the physics in the K' valley can be derived by considering time-reversal symmetry. Analytically, the model Hamiltonian reproduces well the dispersions and phase boundaries obtained by full-wave simulations [see Sec. (S2)]. In Sec. (S3) we present an analytical derivation of the topological indices for different acoustic valley Hall insulators, accompanied with their numerical verifications in Sec. (S4).

### S1. Effective Hamiltonian for bilayer sonic crystals

Firstly, we give a brief summary on the k·p model introduced previously for describing a monolayer sonic crystal [1,2]. For a monolayer sonic crystal made of a hexagonal array of regular triangular scatterers with rotation angle  $\gamma = 0$ , the system has  $C_{3v}$  symmetry and supports deterministic double degeneracy at the Brillouin zone corners. Together with the symmetry analysis, the perturbation Hamiltonian contributes linear dispersions (of slopes  $\pm v_D$ ) near the Dirac frequency  $\omega_D$ . Once the triangular scatterers are slightly rotated, the conic degeneracy at K point is lifted and a perturbation Hamiltonian can be generally written as

$$\delta H'_{\text{MSC}} = \begin{pmatrix} \omega_{p^-}^2 - \omega_D^2 & 2\omega_D v_D (\kappa_x - i\kappa_y) \\ 2\omega_D v_D (\kappa_x + i\kappa_y) & \omega_{q^+}^2 - \omega_D^2 \end{pmatrix}, \quad (\text{S1})$$

where the base functions are selected as the degenerate acoustic valley vortex states  $\{\psi_{p^-}^0, \psi_{q^+}^0\}$  for  $\gamma = 0$ ,  $\omega_i$  with  $i = \{p^+, q^-\}$  represents the frequencies of the nondegenerate acoustic valley vortex states for  $\gamma \neq 0$ , and  $(\kappa_x, \kappa_y)$  describes the wavevector deviated from the K point. The mass terms  $\omega_{p^-}^2 - \omega_D^2 \approx 2\eta\omega_D\gamma$  and  $\omega_{q^+}^2 - \omega_D^2 \approx -2\eta\omega_D\gamma$  are proportional to the (small) rotation angle  $\gamma$ , where the coefficient  $\eta$  can be extracted from the angularly dependent bandgap [2]. Interestingly, the coefficient  $\eta$  increases almost linearly with the volume filling ratio of the triangular scatterers.

Now we consider the BSC case. The basis is initially selected as the four eigenstates of the BSC with rotation angles  $\gamma_1 = \gamma_2 = 0$  in the absence of interlayer coupling, i.e.,  $\{\psi_i^0\}$  with  $i = \{p_1^-, q_1^+, p_2^-, q_2^+\}$ , where the additional subscripts 1 and 2 are layer indices. For small values of  $\gamma_1$  and  $\gamma_2$ , the Hamiltonian of the BSC without interlayer coupling is a direct sum of those for independent monolayers,

$$\delta H'_{\text{intra}} = \begin{pmatrix} 2\eta\omega_D\gamma_1 & 2\omega_D v_D(\kappa_x - i\kappa_y) \\ 2\omega_D v_D(\kappa_x + i\kappa_y) & -2\eta\omega_D\gamma_1 \end{pmatrix} \oplus \begin{pmatrix} 2\eta\omega_D\gamma_2 & 2\omega_D v_D(\kappa_x - i\kappa_y) \\ 2\omega_D v_D(\kappa_x + i\kappa_y) & -2\eta\omega_D\gamma_2 \end{pmatrix}.$$

Considering the interlayer coupling, a new basis can be selected as the linear combination of the original one, i.e.,

$$\begin{cases} \psi_{p,S}^0 = (\psi_{p_1^-}^0 + \psi_{p_2^-}^0) / \sqrt{2} \\ \psi_{p,A}^0 = (\psi_{p_1^-}^0 - \psi_{p_2^-}^0) / \sqrt{2} \end{cases} \text{ and } \begin{cases} \psi_{q,S}^0 = (\psi_{q_1^+}^0 + \psi_{q_2^+}^0) / \sqrt{2} \\ \psi_{q,A}^0 = (\psi_{q_1^+}^0 - \psi_{q_2^+}^0) / \sqrt{2} \end{cases},$$

where the subscripts  $S$  and  $A$  describe the symmetric and antisymmetric with respect to horizontal reflection  $\sigma_h$ . The reflection operator, satisfying  $\sigma_h^2 = 1$ ,  $\sigma_h \psi_{p_1^-}^0 = \psi_{p_2^-}^0$ , and  $\sigma_h \psi_{q_1^+}^0 = \psi_{q_2^+}^0$ , is an element of  $D_{3h}$ , which is the point group for the BSC with  $\gamma_1 = \gamma_2 = 0$ . In this new basis, the BSC Hamiltonian with interlayer coupling is diagonalized with diagonal items  $\{\omega_{p,S}^2, \omega_{p,A}^2, \omega_{q,S}^2, \omega_{q,A}^2\}$ . Due to the equivalence of  $p$  and  $q$ ,  $\omega_{p,S} = \omega_{q,S} \equiv \omega_S$  and  $\omega_{p,A} = \omega_{q,A} \equiv \omega_A$ . Thus in the original basis, the perturbation term for the interlayer coupling reads

$$\delta H'_{\text{inter}} = \begin{pmatrix} 0 & 0 & -\omega_D \Delta\omega_{AS} & 0 \\ 0 & 0 & 0 & -\omega_D \Delta\omega_{AS} \\ -\omega_D \Delta\omega_{AS} & 0 & 0 & 0 \\ 0 & -\omega_D \Delta\omega_{AS} & 0 & 0 \end{pmatrix},$$

where  $\Delta\omega_{AS} = (\omega_A^2 - \omega_S^2) / 2\omega_D \approx \omega_A - \omega_S$  is the frequency bandgap between the anti-symmetric and symmetric modes. Note that here the scatterer rotation is not taken into account for the interlayer coupling since it is quadratic small to the eigenfrequency. Combining the intralayer and interlayer couplings together, we get the total perturbation Hamiltonian for the BSC (scaled by  $2\omega_D$ ), i.e.,  $\delta H = (\delta H'_{\text{intra}} + \delta H'_{\text{inter}}) / 2\omega_D$ , which satisfies the eigen equation  $\delta H \psi = \delta \omega \psi$  with  $\delta \omega$  being the frequency deviation to  $\omega_D$ .

Utilizing the Pauli matrices,  $\sigma_i$  for valley pseudospins and  $s_i$  for layer pseudospins, the perturbation Hamiltonian [i.e., Eq. (1) in the main text] can be concisely written as

$$\delta H = v_D (\kappa_x \sigma_x + \kappa_y \sigma_y) + \eta (\alpha s_z + \beta) \sigma_z - \Delta_c s_x, \quad (\text{S2})$$

where  $\alpha = (\gamma_1 - \gamma_2)/2$ ,  $\beta = (\gamma_1 + \gamma_2)/2$  and  $\Delta_c = \Delta \omega_{AS}/2$ . Specifically,  $\eta \alpha s_z \sigma_z$  mimics the spin-orbit coupling in quantum spin Hall effect and  $\Delta_c s_x$  mimics a Zeeman term in electronic systems. For the BSCs involved in the main text, three parameters are numerically extracted:  $v_D = 0.643$ ,  $\eta = 0.0036/\text{deg}$ , and  $\Delta_c = 0.0206$ , where the former two depend on the filling ratio of the triangular scatterers and the third one depends mostly on the geometry of the penetrated holes that connect the double layers.

## S2. Analytical dispersion curves and phase boundaries

For brevity, we use the substitutions  $v_D \kappa_x / \eta = k_x$ ,  $v_D \kappa_y / \eta = k_y$  and  $\Delta_c / \eta = h$  to rewrite the Hamiltonian as  $\delta H = \eta [(k_x \sigma_x + k_y \sigma_y) + (\alpha s_z + \beta) \sigma_z - h s_x]$ . Solving the eigen problem  $\delta H \phi_n = \delta \omega_n \phi_n$  in the cylindrical coordinates  $(k, \theta)$ , with  $k = \sqrt{k_x^2 + k_y^2}$  and  $\theta = \arg(k_x + ik_y)$ , we obtain dispersion curves for the four bands:  $\delta \omega_{1,2} = -\eta f_{1,2}$  and  $\delta \omega_{3,4} = \eta f_{2,1}$ , where the subscript labels the bands orderly, and  $f_{1,2} = \sqrt{k^2 + h^2 + \alpha^2 + \beta^2 \pm 2\chi}$  with  $\chi = \sqrt{\alpha^2 \beta^2 + \beta^2 h^2 + h^2 k^2}$ . Figure S1(a) presents the analytical dispersions (blue dots) for several typical BSCs mentioned in the main text. The excellent agreements with the simulated results (red lines) validate the effectiveness of our analytical model, even for the BSCs with relatively large rotation angles. In addition, the eigen problem gives the corresponding eigenstates  $\phi_n = N_n^{-1} (a_n, b_n e^{i\theta}, c_n, d_n e^{i\theta})^T$ , with  $N_n = \sqrt{a_n^2 + b_n^2 + c_n^2 + d_n^2}$  being normalization factors. Specifically, here we present explicit forms for the  $k$ -dependent coefficients of the first two bands,

$$\begin{cases} a_1 = h^2\beta + (\alpha\beta + \chi)(\alpha + \beta - f_1) \\ b_1 = k(h^2 + \alpha\beta + \chi) \\ c_1 = -h(k^2 + \beta^2 + \chi - \beta f_1) \\ d_1 = -hk(\alpha - f_1) \end{cases} \quad \text{and} \quad \begin{cases} a_2 = h^2\beta + (\alpha\beta - \chi)(\alpha + \beta - f_2) \\ b_2 = k(h^2 + \alpha\beta - \chi) \\ c_2 = -h(k^2 + \beta^2 - \chi - \beta f_2) \\ d_2 = -hk(\alpha - f_2) \end{cases},$$

which will be used to evaluate the topological invariants below.

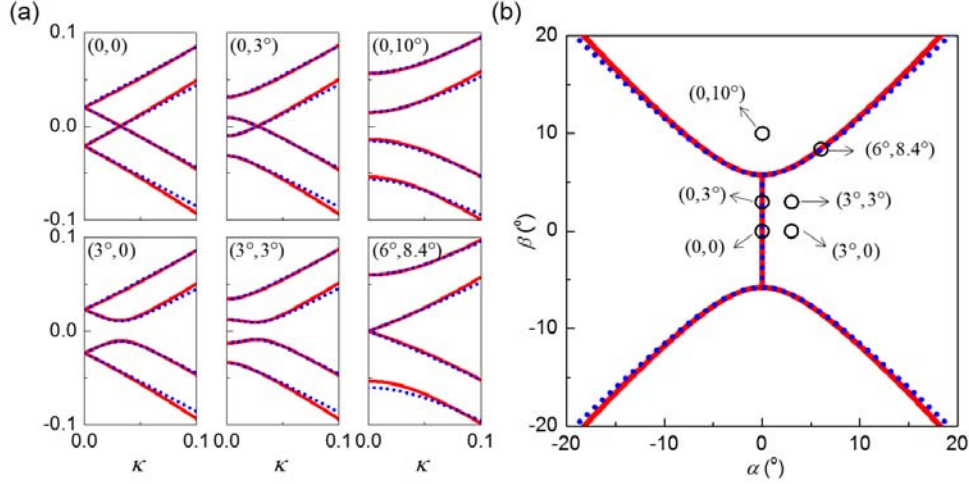


FIG. S1. (a) Dispersions near the K point for the BSCs with different rotation angles. (b) Phase boundaries around the point  $(\alpha, \beta) = (0, 0)$ . The BSC systems concerned in (a) are marked by the black circles in (b). In both (a) and (b), the analytical data (blue dots) capture well the results obtained by COMSOL simulations (red lines).

The analytical model can also predict the phase boundary precisely. As stated in the main text, the topological phase transition is accompanied with the closure of the omnidirectional bandgap between the inner two bands, i.e., the 2<sup>nd</sup> and 3<sup>rd</sup> ones. This requires  $\delta\omega_2 = \delta\omega_3$  and thus  $f_2 = 0$ , which gives rise to

$k = \sqrt{h^2 - \alpha^2 - \beta^2 \pm 2\sqrt{\alpha^2(\beta^2 - h^2)}}$ . To obtain real solution of  $k$ , the conditions  $\alpha = 0$  or  $\beta^2 \geq h^2$  must be satisfied. For the case of  $\alpha = 0$ , we have the solution  $k = \sqrt{h^2 - \beta^2}$  with  $-h \leq \beta \leq h$ . This gives the straight phase boundary in Fig. S1(b), which corresponds to the gap closure associated with nodal ring degeneracy. For the case of  $\beta^2 \geq h^2$ , we have  $k = \sqrt{-(\sqrt{\beta^2 - h^2} \pm |\alpha|)^2}$ , leading to the solution  $k = 0$

with  $\beta = \pm\sqrt{h^2 + \alpha^2}$ . This corresponds to the curved phase boundaries in Fig. S1(b), associated with accidental Dirac point degeneracy. Note that although the perturbation Hamiltonian is established in the vicinity of  $(\alpha, \beta) = (0, 0)$ , it works well within a relatively wide angular range, which is verified in Fig. S1(b) by the excellent agreement between the analytical (blue dots) and simulated (red lines) phase boundaries.

### S3. Layer-polarized valley Chern numbers and topological invariants

Below we present an analytical derivation for the quantized topological invariants. To distinguish all topological phases emerging in Fig. 2(b) (see main text), both the valley and layer pseudospins involved in the Hamiltonian must be resolved. Here we introduce layer-polarized valley Chern numbers (VCNs)  $C_{\pm}^K$  to describe the two bands below the omnidirectional bandgap, where the signs  $+$  and  $-$  correspond to the regrouped states confined in the upper and lower layers, respectively. The approach, which has been developed in electronic systems [3-6], is briefly depicted below.

To calculate the layer-polarized VCNs, the Hamiltonian is projected into a layer pseudospin subspace, where the operator  $s_z = \text{diag}\{1, -1\}$  carries eigenvalues  $+1$  and  $-1$  for the upper and lower layer-polarized states. Spanning  $s_z$  in the basis  $\{\phi_1, \phi_2\}$  of the lower two bands, a 2D matrix  $\langle \phi_i | s_z | \phi_j \rangle = [m_{11}, m_{12}; m_{21}, m_{22}]$  is obtained, where the components  $m_{11} = -m_{22} = m$  and  $m_{12} = m_{21} = t$  with  $m = N_1^{-2}(a_1^2 + b_1^2 - c_1^2 - d_1^2)$  and  $t = N_1^{-1}N_2^{-1}(a_1a_2 + b_1b_2 - c_1c_2 - d_1d_2)$ . The matrix gives the regrouped eigenstates  $\psi_{\pm} = (\phi_1 \pm \xi^{\pm 1} \phi_2) / \sqrt{1 + \xi^{\pm 2}}$  with  $\xi = t^{-1}(\sqrt{m^2 + t^2} - m)$ , whose polarizabilities are characterized by the corresponding eigenvalues  $\lambda_{\pm} = \pm\sqrt{m^2 + t^2}$ . Note that the existence of the polarization spectral gap,  $\Delta\lambda = \lambda_+ - \lambda_-$ , guarantees the effectiveness of the definition for the layer-polarized VCNs.

The layer-polarized VCNs can be evaluated by an integral over the whole K

valley, i.e.,  $C_{\pm}^K = \frac{1}{2\pi} \iint_{\kappa} \Omega_{\pm}(\kappa, \theta) d\kappa d\theta$ . Here  $\Omega_{\pm}(\kappa, \theta) = 2\kappa^{-1} \text{Im} \langle \partial_{\theta} \psi_{\pm} | \partial_{\kappa} \psi_{\pm} \rangle$  are Berry curvatures defined in the polar coordinates, which are strongly localized around the K point. The definition of the VCNs is similar to the original VCN defined for each band [2], except that here the new basis functions  $\psi_{\pm}$  replace  $\phi_{1,2}$  to evaluate the Berry curvatures. Substituting  $\Omega_{\pm}(\kappa, \theta)$  into the definition of the layer-polarized VCNs, we get

$$C_{\pm}^K = \lim_{k \rightarrow \infty} P_{\pm}(k) - \lim_{k \rightarrow 0} P_{\pm}(k), \quad (\text{S3})$$

with

$$P_{\pm}(k) = (P_1 + \xi^{\pm 2} P_2 \pm 2\xi^{\pm 1} Q) / (1 + \xi^{\pm 2}) \quad (\text{S4})$$

being the azimuthal connections defined by  $\psi_{\pm}$ . More specifically,  $P_{1,2} = i \langle \phi_{1,2} | \partial_{\theta} \phi_{1,2} \rangle = -N_{1,2}^{-2} (b_{1,2}^2 + d_{1,2}^2)$ ,  $Q = i \langle \phi_1 | \partial_{\theta} \phi_2 \rangle = -N_1^{-1} N_2^{-1} (b_1 b_2 + d_1 d_2)$ , and the coefficient  $\xi = t^{-1} (\sqrt{m^2 + t^2} - m)$ .

To obtain the layer-polarized VCNs, we need to calculate the limits of  $P_{\pm}(k)$  at  $k=0$  and  $\infty$  points. Consider the limits of  $P_{1,2}(k)$  first. As  $k \rightarrow \infty$ ,  $\chi = |h|k$  and  $f_{1,2} = k$  to the leading order, and thus the coefficients of the eigenstates  $a_{1,2} = \mp |h|k^2$ ,  $b_{1,2} = \pm |h|k^2$ ,  $c_{1,2} = -hk^2$ ,  $d_{1,2} = +hk^2$ , and  $N_{1,2} = 2|h|k^2$ . This gives  $P_{1,2}(\infty) = -1/2$ . The limit calculation at  $k=0$  is relatively complicate. As  $k \rightarrow 0$ ,  $a_{1,2} = h^2 \beta + (\alpha \beta \pm \chi)(\alpha + \beta - f_{1,2})$ ,  $b_{1,2} = k(h^2 + \alpha \beta \pm \chi)$ ,  $c_{1,2} = -h(\beta^2 \pm \chi - \beta f_{1,2})$ , and  $d_{1,2} = -hk(\alpha - f_{1,2})$  to the leading order, where  $\chi = |\beta| \sqrt{\alpha^2 + h^2}$  and  $f_{1,2} = \left| \sqrt{\alpha^2 + h^2} \pm |\beta| \right|$ . For example,  $b_1(0) \equiv d_1(0) \equiv 0$ , and  $a_1(0)$  and  $c_1(0)$  are nonzero only if  $\beta < 0$ . Therefore, it is easy to derive  $P_1(0) = 0$  for  $\beta < 0$ , and for  $\beta > 0$ ,

$$P_1(0) = -\lim_{k \rightarrow 0} \frac{b_1^2 + d_1^2}{N_1^2} = -\lim_{k \rightarrow 0} \frac{b_1 b_1' + d_1 d_1'}{a_1 a_1' + b_1 b_1' + c_1 c_1' + d_1 d_1'} = -\lim_{k \rightarrow 0} \frac{b_1' b_1' + d_1' d_1'}{b_1' b_1' + d_1' d_1'} = -1,$$

where the L'Hôpital's rule has been applied associated with the derivatives  $a_1'(0) = c_1'(0) = 0$ . Similarly,  $P_2(0) = 0$  for  $0 < \beta < \sqrt{h^2 + \alpha^2}$  and  $\beta < -\sqrt{h^2 + \alpha^2}$ ,

and  $P_2(0) = -1$  for  $-\sqrt{h^2 + \alpha^2} < \beta < 0$  and  $\beta > \sqrt{h^2 + \alpha^2}$ .

Now we focus on the quantities  $Q$  and  $\xi$  around point  $O_1$  in the phase diagram, and give  $P_{\pm}(k)$ ,  $C_{\pm}^K$  and the topological invariants finally. Again, by expanding the coefficients to the first order, it is easy to obtain the behaviors at  $k \rightarrow \infty$ , i.e.,  $t(\infty) = -1$ ,  $m(\infty) = 0$  and  $Q(\infty) = 0$ , such that  $\xi(\infty) = -1$  and  $P_{\pm}(\infty) = -1/2$ . At the limit  $k \rightarrow 0$ , it can be proven that  $Q(0) = 0$  and thus  $P_{\pm}(0) = [P_1(0) + \xi^{\pm 2}(0)P_2(0)]/[1 + \xi^{\pm 2}(0)]$ . Therefore,  $P_{\pm}(0) = \pm 1$  for the region  $\beta > \sqrt{h^2 + \alpha^2}$ , and  $P_{\pm}(0) = 0$  for the region  $\beta < -\sqrt{h^2 + \alpha^2}$ , or more briefly,  $P_{\pm}(0) = -(1 \pm \text{sgn } \beta)/2$  for  $|\beta| > \sqrt{h^2 + \alpha^2}$ . On the other hand,  $P_{\pm}(0) = -1/[1 + \xi^{\pm 2}(0)]$  for the region  $0 < \beta < \sqrt{h^2 + \alpha^2}$ , and  $P_{\pm}(0) = -\xi^{\pm 2}(0)/[1 + \xi^{\pm 2}(0)]$  for the region  $-\sqrt{h^2 + \alpha^2} < \beta < 0$ . Take the first case as an example. Utilizing the L'Hôpital's rule, we can prove that, for  $\alpha > 0$ ,  $\xi(0) = 0$  and thus  $P_+(0) = -1$  and  $P_-(0) = 0$ ; for  $\alpha < 0$ ,  $\xi^{-1}(0) = 0$  and thus  $P_+(0) = 0$  and  $P_-(0) = -1$ . This can be summarized as  $P_{\pm}(0) = -(1 \pm \text{sgn } \alpha)/2$  for the region  $0 < \beta < \sqrt{h^2 + \alpha^2}$ . A similar analysis gives the same result for the other case with  $-\sqrt{h^2 + \alpha^2} < \beta < 0$ . Therefore, we have  $P_{\pm}(0) = -(1 \pm \text{sgn } \alpha)/2$  for the region  $|\beta| < \sqrt{h^2 + \alpha^2}$ . Eventually, the layer-polarized VCN distributions can be concluded:

$C_{\pm}^K = \pm \frac{\text{sgn } \alpha}{2}$  for  $|\beta| < \sqrt{h^2 + \alpha^2}$ , and  $C_{\pm}^K = \frac{\text{sgn } \beta}{2}$  for  $|\beta| > \sqrt{h^2 + \alpha^2}$ . As explicitly labeled in the phase diagram [see Fig. 2(b) in the main text], two types of quantized topological invariants can be defined to characterize the valley-projected topological phases, i.e.,  $C_V^K = C_+^K + C_-^K$  and  $C_L^K = C_+^K - C_-^K$ . The former is a natural bilayer extension of the VCN concerned in the monolayer system [2], and the latter identifies the layer information and resembles that proposed for QSH systems. Specifically, we have  $C_V^K = \text{sgn}(\beta)$  and  $C_L^K = 0$  for the phase region  $|\beta| > \sqrt{h^2 + \alpha^2}$ , while  $C_L^K = \text{sgn}(\alpha)$  and  $C_V^K = 0$  for the phase region  $|\beta| < \sqrt{h^2 + \alpha^2}$ .

Any interface that separates two topologically distinct BSCs can host edge states. In the main text we have demonstrated the most fundamental interface systems, constructed either by two different AVH phases or by two different ALH phases. As a complement, here we provide the projected dispersions for another two representative systems. The first one consists of two BSCs with rod orientations  $(10^\circ, 3^\circ)$  and  $(10^\circ, -3^\circ)$ . Figure S2(a) shows the corresponding interface dispersion. As predicted, there is no any edge state emerging in the bulk gap, since both BSCs belong to topologically identical ALH phases. The second interface system is constructed by the BSCs with rod orientations  $(0, 20^\circ)$  and  $(10^\circ, 3^\circ)$ , belonging to AVH and ALH phases respectively. The projected dispersion shows a time-reversal pair of edge states, since the difference of the topological invariants across the interface is 1.

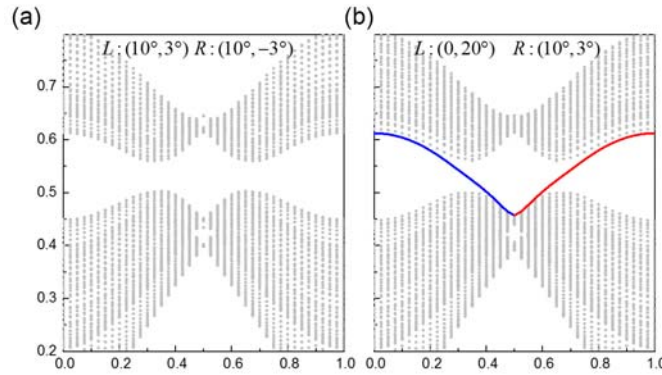


FIG. S2. Projected dispersions along an interface separating two topologically identical BSCs (a), and two topologically distinct BSCs with AVH and ALH phases respectively (b). The red and blue curves in (b) correspond to the edge modes projected by the K and K' valleys.

#### S4. Numerical verifications for the layer-polarized VCNs and topological invariants

To check the analytical derivation made in previous section, we have also numerically calculated the layer-polarized VCNs near the  $O_1$  point based on the definition  $C_{\pm}^K = \iint_K d\kappa^2 \Omega_{\pm}(\kappa, \theta)/2\pi$ . This further gives the topological invariants  $C_L^K$  and  $C_V^K$ . The numerical data are provided in Figs. S3(a)-S3(d), which are consistent with the analytical results mentioned above. Similarly, Figs. S3(e)-S3(h) provide the numerical data for the BSC around the  $O_2$  point. Note that for the  $O_2$  case,

the inversion symmetry replaces the horizontal mirror symmetry, and the configuration for the upper layer is rotated by  $60^\circ$  leading to a sign-inversed  $\eta$  for that layer. As a consequence, the perturbation Hamiltonian around the K valley can be written as [7]

$$\delta H = v_D(\kappa_x \sigma_x + \kappa_y \sigma_y) - \eta(\beta s_z + \alpha) \sigma_z - \Delta_c s_x. \quad (\text{S5})$$

Here  $\Delta_c$  is the frequency difference between the antisymmetric and symmetric modes under inversion symmetry, and now  $(\alpha, \beta)$  are rotation angles with respect to the reference point  $O_2$ .

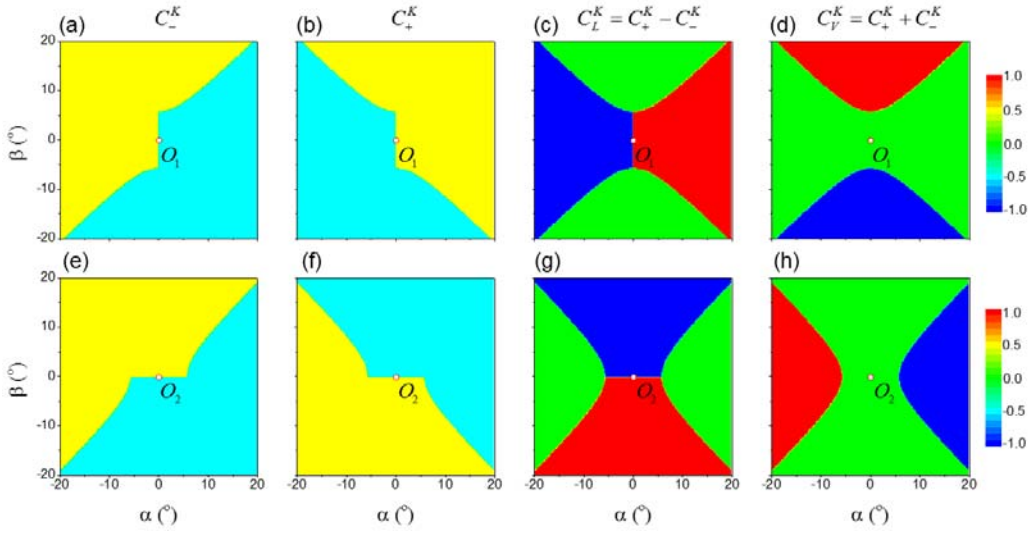


FIG. S3. (a) and (b): Numerical distributions of the layer-polarized VCNs  $C_{\pm}^K$  for the BSCs near the  $O_1$  point. (c) and (d): The corresponding topological invariants  $C_L^K$  and  $C_V^K$ . (e)-(h): Similar to (a)-(d), but for the BSCs near the  $O_2$  point.

## References

- [1] J. Lu, C. Qiu, S. Xu, Y. Ye, M. Ke, and Z. Liu, *Dirac cones in two-dimensional artificial crystals for classical waves*. Phys. Rev. B **89**, 134302 (2014).
- [2] J. Lu, C. Qiu, L. Ye, X. Fan, M. Ke, F. Zhang, and Z. Liu, *Observation of topological valley transport of sound in sonic crystals*. Nature Physics **13**, 369 (2017).
- [3] E. Prodan, *Robustness of the spin-Chern number*. Phys. Rev. B **80**, 125327 (2009).
- [4] Y. Yang, Z. Xu, L. Sheng, B. Wang, D. Y. Xing, and D. N. Sheng, *Time-reversal-symmetry-broken quantum spin Hall effect*. Phys. Rev. Lett. **107**, 066602 (2011).
- [5] H. Li, L. Sheng, D. N. Sheng, and D. Y. Xing, *Chern number of thin films of the topological insulator  $\text{Bi}_2\text{Se}_3$* . Phys. Rev. B **82**, 165104 (2010).
- [6] W.-Y. Shan, H.-Z. Lu, and S.-Q. Shen, *Effective continuous model for surface states and thin films of three-dimensional topological insulators*. New J. Phys. **12**, 043048 (2010).
- [7] The model Hamiltonians around the  $O_3$  and  $O_4$  points can be derived similarly.